Protein Science (1999), *8*:2598–2610. Cambridge University Press. Printed in the USA.

Rotamer strain as a determinant of protein structural specificity

GREG A. LAZAR,[1] ERIC C. JOHNSON,[1,2] JOHN R. DESJARLAIS,[3] AND TRACY M. HANDEL[1]

[1]Department of Molecular and Cell Biology, Stanley Hall, University of California, Berkeley, California 94720
[2]Department of Physics, University of California, Berkeley, California 94720
[3]Department of Chemistry, Chandlee Laboratory, Penn State University, University Park, Pennsylvania 16802

(RECEIVED June 29, 1999; ACCEPTED September 24, 1999)

Abstract

We present direct evidence for a change in protein structural specificity due to hydrophobic core packing. High resolution structural analysis of a designed core variant of ubiquitin reveals that the protein is in slow exchange between two conformations. Examination of side-chain rotamers indicates that this dynamic response and the lower stability of the protein are coupled to greater strain and mobility in the core. The results suggest that manipulating the level of side-chain strain may be one way of fine tuning the stability and specificity of proteins.

Keywords: hydrophobic core; NMR; packing; protein design; rotamer; specificity; strain; ubiquitin

Natural proteins have levels of structural specificity that span an enormous range—from highly flexible and comformationally promiscuous, unfolded, or partially folded states to rigid compact structures. It is generally accepted that the degree of structural specificity is related to protein function, whether that function is signal transduction, binding/transport, or catalysis. Important insights into the relationship between conformational flexibility and function are emerging from crystallographic studies (Rader & Agard, 1997; Harata et al., 1999), NMR dynamics experiments (Palmer, 1997), normal mode calculations (Anderson et al., 1997; Miller & Agard, 1999), and molecular dynamics simulations (Chatfield et al., 1998; Philippopoulos & Lim, 1999). Equally important will be to understand how various energetic interactions determine the conformational states accessible to proteins.

Protein design is an extremely powerful approach for addressing such questions. Until recently, the design of a protein with a high degree of structural specificity had not been demonstrated, making this a major goal in the field. The application of computational methods to design has reversed this trend, and recently many successes have been reported including the design of novel hydrophobic cores (Lazar & Handel, 1998), metal binding sites (Hellinga, 1998), and complete de novo proteins (Dahiyat & Mayo, 1997; Kortemme et al., 1998; Walsh et al., 1999). With these developments, our prediction is that the new hurdles in the field will be to engineer function and binding. As efforts shift from designing stable, well-ordered protein scaffolds to functional proteins, a more refined understanding of what interactions control structure, stability, and specificity will be necessary.

We have focused on understanding the role of hydrophobic core packing in proteins. Our approach couples systematic computational methods with detailed experimental investigation of designed proteins. We previously developed the program ROC (Repacking of Cores) (Desjarlais & Handel, 1995) and used it to design a number of ubiquitin variants that span a wide range of stabilities (Lazar et al., 1997). The objective of the present study was to investigate the structure and dynamics of one of these variants, 1D8, which has eight hydrophobic core mutations relative to the wild-type (WT) protein: I3L, I13L, L15V, V17L, I23V, V26L, I61L, and L67I. This variant has the same core volume as WT, but is destabilized by 2.6 kcal/mol. To characterize this protein, NMR was the structural method of choice because of its sensitivity to conformational flexibility. Structural and dynamic data indicate that 1D8 is in slow exchange between two states and has less defined side-chain structure than WT. To understand why the new core results in increased dynamic behavior and lower stability in 1D8, we carefully analyzed the side chain conformations using computational and statistical methods. To assess the extent to which packing can affect structural specificity, we also characterized R7, a variant with a randomized WT core. The results illustrate some general principles that are relevant to both natural and designed proteins.

Reprint requests to: Tracy M. Handel, Department of Molecular and Cell Biology, University of California, Berkeley c/o Stanley/Donner Administrative Services Unit, 229 Stanley Hall, Berkeley, California 94720; e-mail: handel@paradise1.berkeley.edu.

Abbreviations: 2D, 3D, 4D, two-, three-, and four-dimensional; CD, circular dichroism; HMQC, heternouclear multiple quantum coherence; HSQC, heteronuclear single quantum coherence; NOE, nuclear Overhauser effect; NOESY, nuclear Overhauser effect spectroscopy; WT, wild-type.

Results and discussion

Assignment and structure of 1D8

The solution structure of 1D8 was solved with standard three- and four-dimensional heteronuclear NMR methods. Figure 1A shows a stereoview of the backbone superposition of the 20 lowest energy structures in the final round of calculations. The ensemble is well-defined with a root-mean-square deviation (RMSD) over the ordered region (residues 1 to 71) of 0.41 Å for backbone atoms and 0.85 Å for all heavy atoms. The number of restraints and structural statistics also reflect the high quality of the structures (Table 1). Backbone superposition of the 1D8 structure closest to the mean with the WT crystal structure (Alexeev et al., 1994) (Fig. 1B) indicates that the backbone conformation is essentially the same (RMSD = 0.69 Å). Identical RMSDs are obtained when 1D8 is compared with the other available WT crystal (Vijay-Kumar et al., 1987) and solution (Cornilescu et al., 1998) structures. The similarity between the design and WT confirms the program ROC's ability to predict alternative core sequences that maintain the backbone structure of a protein. As will be shown, however, analysis of additional NMR data and features of the structures reveals local differences between the proteins.

Table 1. *Experimental restraints and structural statistics*[a] *for 1D8*

Number of experimental restraints	First round	Final round
NOE distance restraints[b]		
Ambiguous	3,244	1,115
Unambiguous	870	2,097
Intraresidue	178	421
Sequential	31	140
Medium range ($2 \leq [i-j] \leq 4$)	74	193
Long range ($[i-j] > 4$)	587	1,343
H-bond[c]		68
Dihedral restraints from coupling constants		84
RMSDs from experimental data		
Average distance restraint violation	0.0054 ± 0.0008 Å	
Average dihedral angle restraint violation	0.043 ± 0.022°	
RMSDs from ideal stereochemistry		
Bonds	0.00087 ± 0.00002 Å	
Angles	0.308 ± 0.002°	
Impropers	0.110 ± 0.004°	
Ramachandran statistics[d] (residues 1–71)		
Residues in most favored regions	82.9%	
Residues in additionally allowed regions	16.4%	
Residues in generously allowed regions	0.7%	
Residues in disallowed regions	0.0%	
Coordinate precision (residues 1–71)		
Backbone	0.41 Å	
Heavy atoms	0.85 Å	

[a] The statistics are for the 20 lowest energy structures from an ensemble of 30 calculations.

[b] The difference in number of ambiguous and unambiguous NOEs at the start and end of the calculation is due to trimming of the assignment possibilities based on distance filtration and percent contribution to the NOE intensity using the ARIA methodology of Nilges (Nilges, 1995; Nilges et al., 1997).

[c] For each of the identifiable 34 H-bonds, two restraints were applied: $1.7 \leq D_{H\text{-}O} \leq 2.2$ Å and $2.7 \leq D_{N\text{-}O} \leq 3.2$ Å.

[d] Ramachandran analysis was calculated with Procheck-NMR (Laskowski et al., 1996).

1D8 is in slow exchange between two conformations

In the process of calculating structures, there were consistent violations that could not be explained by typical problems (spin diffusion, incorrect or missing assignments, truncation, and other spectral artifacts). These violations arose because of the presence of numerous exchange peaks in NOESY spectra. Consequently, we re-examined the $^{15}N/^{1}H$ HSQC spectrum more carefully (Fig. 2A). A second set of peaks of lower intensity was observed. These peaks represent an alternate conformation of 1D8, which is in slow exchange with the major conformation. The stability of 1D8 and the level of dispersion of the smaller peaks, particularly in the ^{1}H dimension (Yao et al., 1997; Dyson & Wright, 1998), indicate that this alternate conformation is not unfolded. The two states of the protein that gives rise to the intense and weak peaks will be referred to as the major and minor conformations, respectively. From peak intensities, the minor conformation corresponds to approximately 5% of the population of the major conformation.

The minor cross peaks were assigned from the exchange peaks in 3D NOESY spectra, and correspondence with the major cross peaks using a 2D heteronuclear correlation experiment (Wider et al., 1991). This is essentially an HSQC with a mixing period inserted after the ^{15}N chemical shift evolution period where longitudinal two-spin order (I_zS_z) is created. Chemical exchange, which occurs during the mixing period, is manifest as a second set of cross peaks that connect the major and minor conformer in a rectangular pattern. Figure 2B shows such an experiment overlaid with the normal $^{15}N/^{1}H$ HSQC. A new set of cross peaks is visible, providing direct correlations between the major and minor conformations. The mixing period in this experiment was varied to determine the optimum delay, which depends on the forward and reverse exchange rates and magnetization relaxation. From these data (not shown), preliminary estimates of the timescale are tens of milliseconds for the minor to major exchange rate and hundreds of milliseconds for the major to minor exchange rate. We also investigated the backbone dynamics of 1D8 and WT ubiquitin using ^{15}N relaxation measurements (data not shown), but standard model-free analysis (Lipari & Szabo, 1982) of the data gave anomalous results and requires further study. Nevertheless, the ^{15}N transverse relaxation times (T2's) of 1D8 are not shorter than those of WT, a result expected if exchange was in the microsecond to millisecond range (Palmer et al., 1996). This is consistent with our slower estimates of the exchange timescale. No minor state was detected in the correlation experiment for WT or another ubiquitin variant, 1D7 (Johnson et al., 1999), using a broad range of mixing times, indicating that the presence of an alternate conformation is thus far unique to 1D8.

Minor 1D8 cross peaks were also observed for side-chain resonances in both ^{15}N-edited (Asn and Gln residues) and ^{13}C-edited spectra. However, because of congestion and the presence of residual water, complete assignment of the minor aliphatic resonances was not possible in the ^{13}C-edited spectra. In well-separated regions clear exchange was observed, in some cases all the way out to core side-chain methyls (Fig. 2C). An interesting result is observed for the two β-protons of Ser65; these have distinct chemical shifts in the major conformation but are degenerate in the minor conformation (Fig. 2D). Although more assignments are necessary

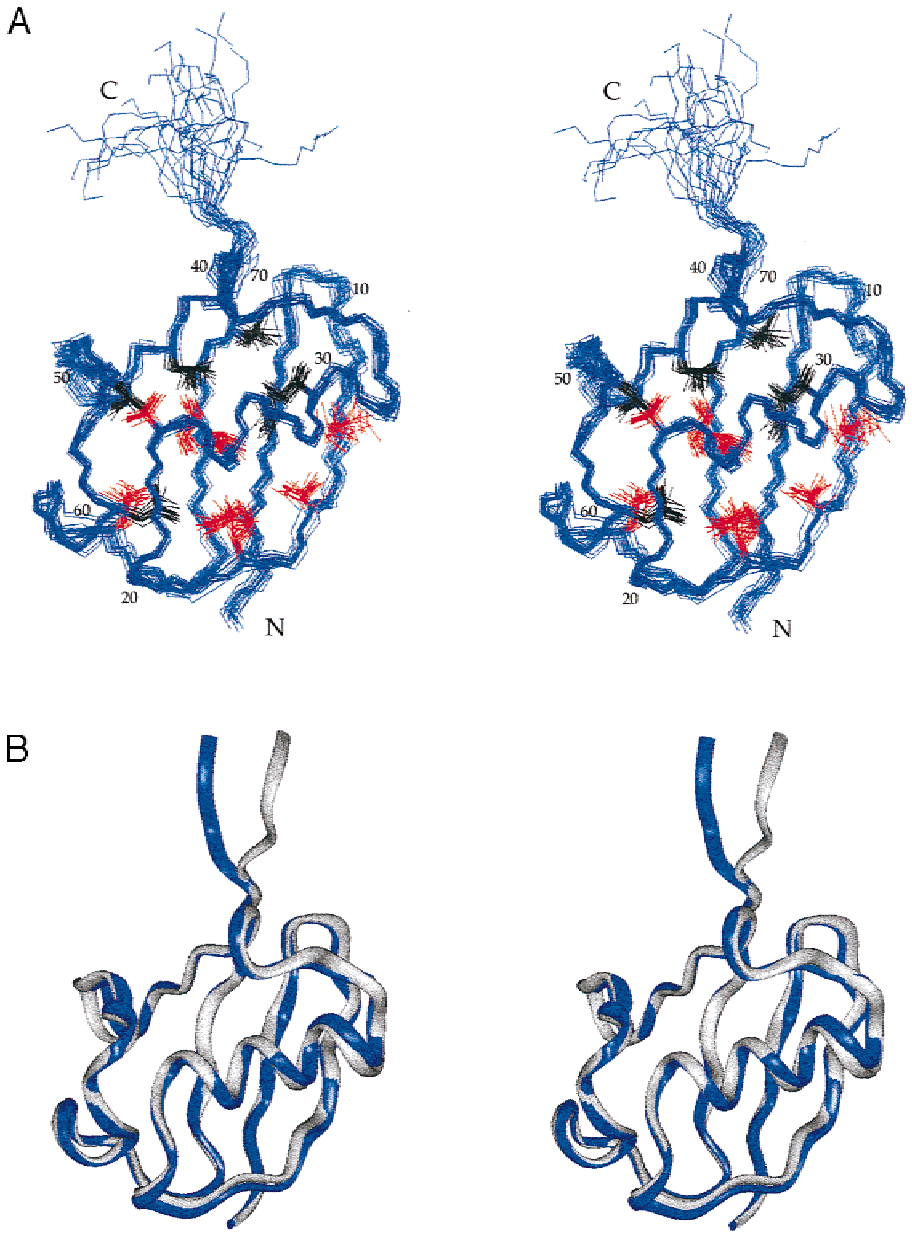

Fig. 1. A: Ensemble of the 20 lowest energy structures of 1D8. Core side chains that are mutated relative to WT are shown in red. Nonmutated core side chains are shown in black. **B:** Superposition of the structures of 1D8 and WT. The 1D8 (blue) structure is closest to the mean in the ensemble, and the WT (gray) is the crystal structure whose coordinates were used for the design (accession code 1UBI (Alexeev et al., 1994)).

to determine the generality of this result, it suggests that, although folded, the minor conformation is more flexible.

There is no NOE data for the minor conformation because the only peaks observed in NOESY spectra are exchange peaks; i.e., no "minor to minor" NOEs are observed. This is presumably due to the low population of this state. However, limited structural information is available from chemical shift assignments. To a first approximation, the degree to which the two conformations differ should be reflected by the magnitude of the chemical shift disparity between them (Fig. 3A,B). In many cases the difference is substantial, as high as 295 Hz (4.9 ppm) in ^{15}N and 935 Hz (1.6 ppm) in ^{1}H. The most significant differences are observed for residues 61–73, which include the last β-strand (β5) and the turn leading into it. The other strands in the sheet also show substantial chemical shift deviations, albeit to a lesser extent than β5. Approximately three-fourths of the molecule (53 of 72 backbone amides) has a minor conformation. In general, residues that do not have an alternate amide conformation reside in loops and turns (Fig. 4). The exception is a set of residues that interact with each other in the most stable elements of secondary structure. Phe4 and Val15 form a hydrogen bond across the β-sheet and show no minor conformation. Val15 packs against Leu26, which along with a

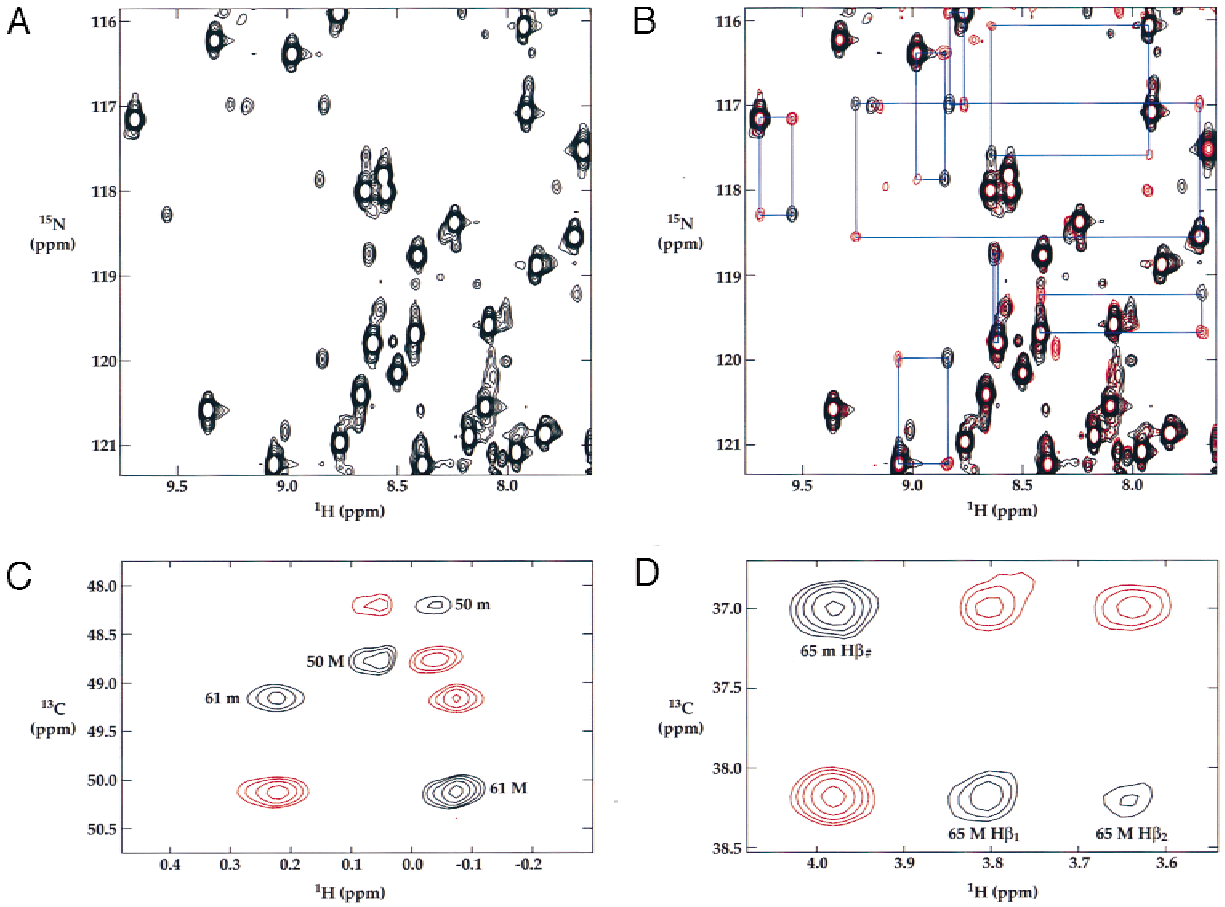

Fig. 2. **A:** Expanded view of a region of the ^{15}N/^{1}H HSQC spectrum of 1D8 contoured at 10σ. Positive and negative (aliased) peaks are both black. **B:** Exchange correlation for the 1D8 protein in the same spectral region as Figure 2A. The black spectrum is the normal ^{15}N/^{1}H HSQC, and the red spectrum is the same experiment with a 125 ms delay immediately following ^{15}N chemical shift evolution. Blue lines indicate exchange correlations by lining up major and minor amide HSQC peaks with correlated exchange cross peaks. **C:** A ^{13}C/^{1}H difference correlation spectrum (Wider et al., 1991), expanded in the region around the δ_2 methyl cross peaks of Leu61 and Leu50. Major (M) and minor (m) cross peaks are positive (black), and exchange correlation cross peaks are negative (red). The difference spectrum was obtained by subtracting two versions of the correlation experiment, one with the mixing time (125 ms) before ^{13}C chemical shift evolution and one with it after. **D:** The same experiment as in Figure 2C, here expanded in the region around the β cross peaks for Ser65. Whereas the two beta protons have nondegenerate resonances in the major conformer (Hβ_1 and Hβ_2), they are degenerate in the minor conformer (H$\beta_\#$).

stretch of residues in the helix (26–29) also show no alternate amide conformation (Fig. 4). It is somewhat peculiar that the C-terminal tail, disordered in the ensemble of structures (Fig. 1A), shows the presence of an alternate conformation all the way to Gly75. This may reflect coupling to the conformation of β5.

Despite the low intensity of the minor peaks in 1D8, the data indicate an important result—core packing has made a single additional conformational state accessible. Exchange between the two states appears to be concerted since a single set of minor cross peaks is observed. These concerted changes propagate from β5 to the rest of the sheet to an extent that falls off with distance from β5 (Fig. 4). The response of the protein to the mutations differs from that observed in most crystallographic studies, which have shown that packing mutants typically relax to a slightly altered yet single backbone conformation (Baldwin et al., 1993; Jackson et al., 1993; Lim et al., 1994). The difference may be due to "freezing out" of a single structure in crystals, differences in the protein folds, or other factors. Previous experiments have shown that packing affects protein specificity (Lim & Sauer, 1991; Starich et al., 1998), and our results suggest that this can occur by shifting the equilibrium between alternate conformations.

Amide exchange protection of 1D8 shows a similar pattern of perturbation

To further investigate local structural and dynamic differences between 1D8 and WT, we measured amide hydrogen/deuterium (H/D) exchange protection (Bai et al., 1995). Assuming an EX2 mechanism, one in which H/D exchange is slow relative to the folding rate of the protein, protection factors directly reflect the equilibrium constant of the unfolding transition or fluctuation required for exchange to occur (Bai et al., 1995). GuHCl-induced unfolding monitored by CD indicates that 1D8 is destabilized relative to WT by approximately 2.6 kcal/mol (Lazar et al., 1997). This translates to an expected loss in protection of two orders of magnitude.

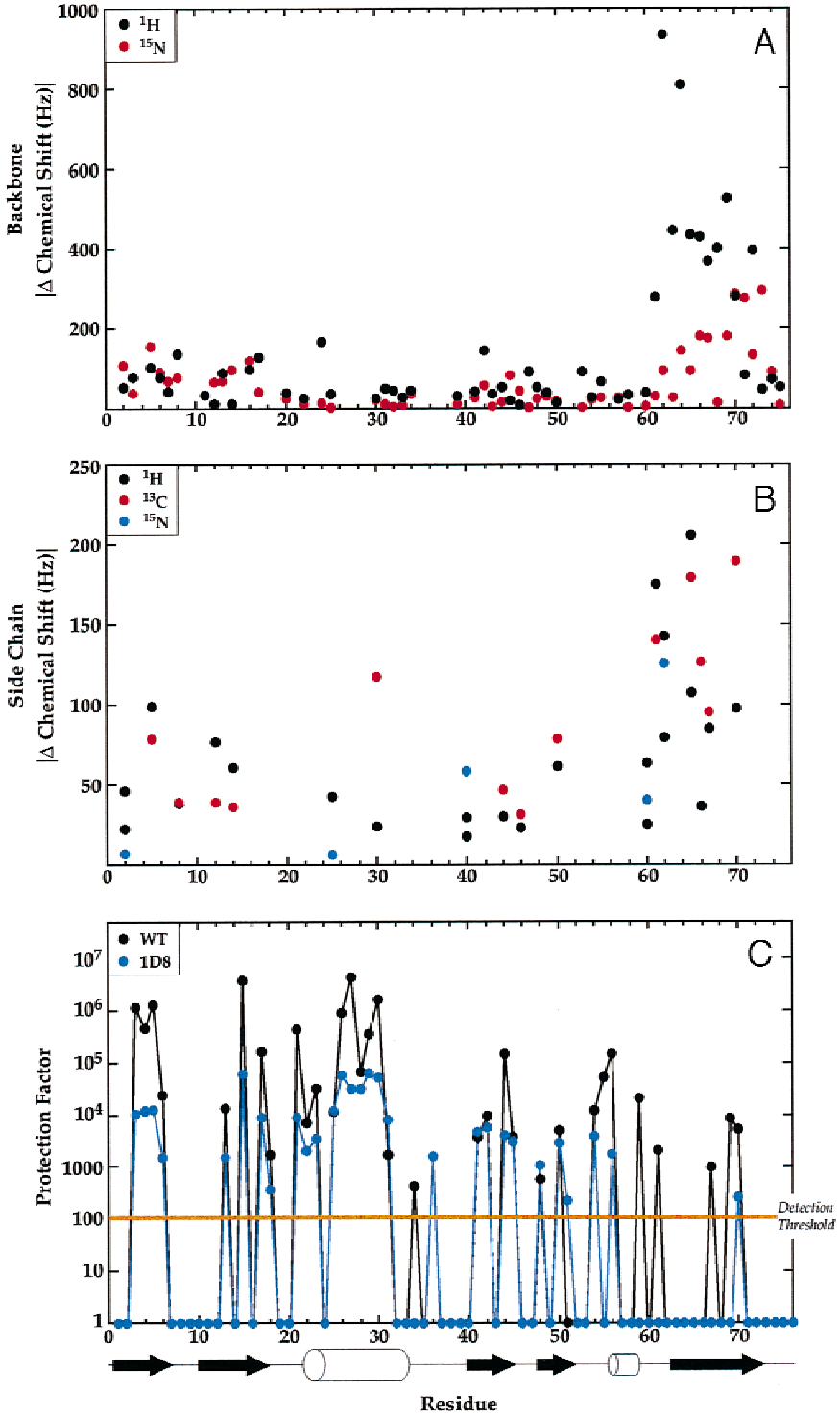

Fig. 3. A: Absolute differences in backbone ^{15}N (black) and amide ^{1}H (red) chemical shifts between the major and minor conformations for each residue. Frequency differences are in Hz. The absence of data for a residue indicates that its amide does not have an alternate conformation. **B:** Absolute differences in side chain ^{1}H (black), ^{13}C (red), and ^{15}N (blue) chemical shifts between the major and minor conformations for a subset of assignable cross peaks. Frequency differences are in Hz. The data represent the following ^{13}C/^{1}H or ^{15}N/^{1}H pairs: Gln2 Nϵ_2/(Hϵ_{21} and Hϵ_{22}), Val5 Cγ_2/H$\gamma_{2\#}$, Leu8 Cδ_2/H$\delta_{2\#}$, Thr12 Cγ_2/H$\gamma_{2\#}$, Thr14 Cβ/Hβ, Asn25 Nδ_2/Hδ_{21}, Ile30 Cδ_1/H$\delta_{1\#}$, Gln40 Nϵ_2/(Hϵ_{21} and Hϵ_{22}), Ile44 Cγ_2/H$\gamma_{2\#}$, Ala46 Cβ/H$\beta_{\#}$, Leu50 Cδ_2/H$\delta_{2\#}$, Asn60 Nδ_2/(Hδ_{21} and Hδ_{22}), Leu61 Cδ_2/H$\delta_{2\#}$, Gln62 Nϵ_2/(Hϵ_{21} and Hϵ_{22}), Ser65 Cβ/(Hβ_1 and Hβ_2), Thr66 Cβ/Hβ, Ile67 Cγ_2/H$\gamma_{2\#}$, 70Val Cγ_2/H$\gamma_{2\#}$. Here the # symbol indicates that the three degenerate protons for methyls, and the methyl carbons for all valines (Cγ_1 and Cγ_2) and leucines (Cδ_1 and Cδ_2) are nondegenerate. **C:** Protection factors for WT (black) and 1D8 (blue). The dashed line at protection factor = 100 indicates the detection limit of the experiment, estimated to be just below the protection factors of the fastest exchanging amides that could be measured. Amides that fall below this limit are set to protection factor = 1 for clarity. Regions of secondary structure are illustrated below the plot.

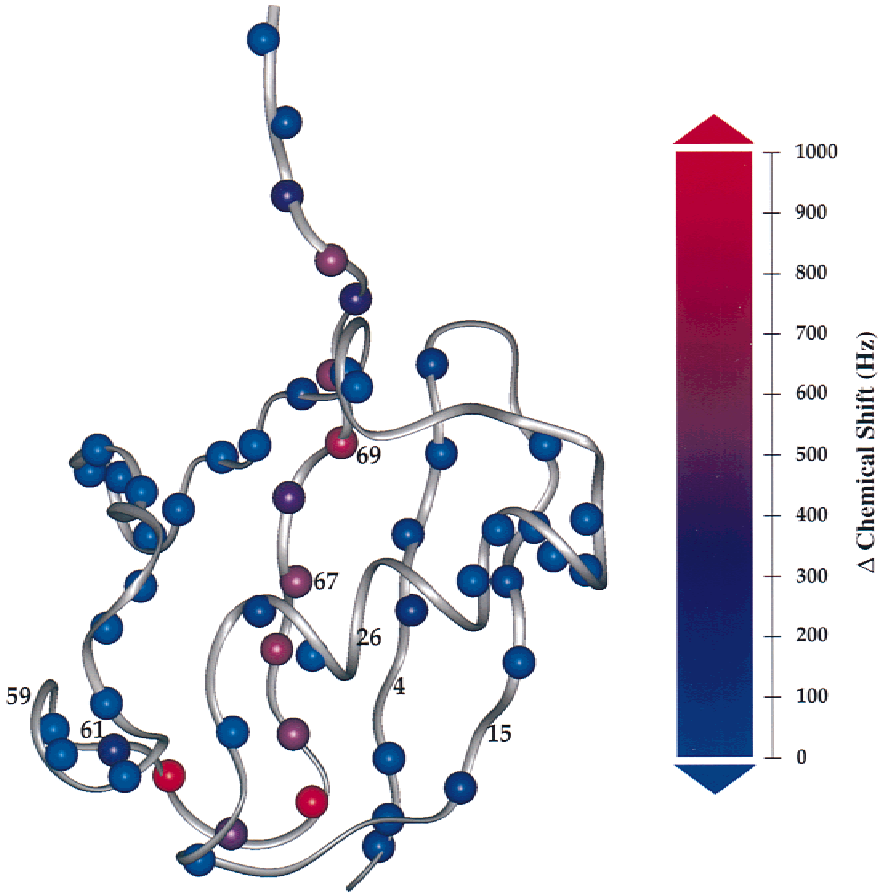

Fig. 4. Chemical shift differences between the major and minor conformations plotted on the structure of 1D8. The color scale represents the summed ^{15}N and ^{1}H frequency differences in Hz from Figure 3A. These data are plotted on the amide nitrogen for each residue. The absence of a sphere for a residue indicates that its amide does not have an alternate conformation. Residues referred to in the text are highlighted: the three in the sheet and helix that do not have a minor amide conformation (4, 15, and 26), and the four that show a loss of amide protection (59, 61, 67, and 69).

Indeed, many amides in 1D8 have protection factors about 100-fold lower than in WT (Fig. 3C). They reside predominantly in the major secondary structure elements of the protein and generally show the highest protection. By contrast, there are several residues that have the same or similar protection factors for WT and 1D8. The majority of these amides are in loops or turns, at the ends of helices or strands, or at the more solvent exposed center position of the α-helix. The results suggest that the less favorable packing in 1D8 primarily affects the global unfolding transition, but has little effect on local fluctuations that do not require unfolding to interact with solvent. This agrees very well with exchange data obtained for the 1D7 variant (Johnson et al., 1999).

An important difference between WT and 1D8 is observed for residues 59–69, involving the last β-strand and the preceding turn. Four amides in this region (59, 61, 67, and 69) show a complete loss of protection. Even after accounting for the global loss in stability, these H-bonds should still be detectable, particularly given that three of the four amides appear to exchange via local fluctuations (Johnson et al., 1999). This, in fact, is the same region of the protein that shows the largest chemical shift differences between the major and minor conformations (Figs. 3, 4). Together, the H/D exchange and chemical shift data strongly suggest that the minor conformation is caused by a structural change primarily involving the last β-strand and the preceding turn in a manner that weakens H-bonds in this region, but according to the chemical shift dispersion does not cause unfolding.

Side-chain rotamer strain is correlated with the change in specificity

At the start of this study our main questions were: (1) how well does ROC do at predicting the side-chain structure of 1D8; and (2) can we understand the lower stability of 1D8 relative to WT? With the observation of the minor conformer that is not observed in WT, we also became interested in understanding the origin of this state, as this information may provide insight into how conformational transitions occur. To address these questions, we examined in detail the predicted and experimentally determined side-chain rotamers of WT and 1D8 (Table 2).

ROC predictions become less accurate with increasing side-chain flexibility

As previously described (Johnson et al., 1999), ROC successfully predicts 12 of 14 side chains for WT ubiquitin, with one

Table 2. *Predicted and experimental rotamers*[a]

	WT											1D8										
			Predicted[c]					Experimental[d]							Predicted[c]					Experimental[d]			
Position	Res	ROC[b]	χ_1	χ_2	%	Rank		χ_1	χ_2	%	Rank	Res[e]	ROC[b]		χ_1	χ_2	%	Rank		χ_1	χ_2	%	Rank
3	I	+	60	180	13	3		60*	180	13	3	**L**	−	(6)	−60	60	8	3		−60*	180*	56	1
														(4)	−60	180	56	1					
5	V	+	180		71	1		180*		71	1	V	+		180		71	1		180*		71	1
13	I	−	60	180	12	3		−60	180	57	1	**L**	?		60	60	1	7		⇔[f]	⇔[f]	R	R
							xtal	130	180	R	R												
15	L	+	−60	180	56	1	(7)	−60	180	56	1	**V**	+		−60		20	2		−60*		20	2
							(3)	−60	−60	2	5												
17	V	+	−60		20	2		−60*		20	2	**L**	−	(5)	60	135	R	R	(7)	−60	180	56	1
														(4)	60	60	1	7	(2)	235	60	R	R
														(1)	−60	113	R	R	(1)	180	60	27	2
23	I	+	−60	−60	16	2		−60*	−60	16	2	**V**	+		180		71	1		180*		71	1
26	V	+	180		71	1		180*		71	1	**L**	+	(9)	180	60	27	2		180*	60*	27	2
														(1)	180	180	4	4					
30	I	+	−60	180	57	1		−60*	180	57	1	I	+		−60	180	57	1		−60*	180	57	1
43	L	+	−60	180	56	1		−60*	180	56	1	L	+		−60	180	56	1		−60*	180*	56	1
50	L	+	−60	180	56	1		−60*	180	56	1	L	+		−60	180	56	1		−60*	180*	56	1
56	L	+	−60	180	56	1		−60*	180	56	1	L	−	(5)	−60	180	56	1		−60*	180*	56	1
														(5)	−60	113	R	R					
61	I	+	−60	180	57	1		−60*	180	57	1	**L**	−	(9)	−60	180	56	1	(5)	−60	−60	8	3
														(1)	180	60	27	2	(4)	−60	180	56	1
																			(1)	−60	126	R	R
67	L	−	−60	180	56	1		−60	60	8	3	**I**	?		−60	180	57	1	(4)	−60*	180	57	1
							xtal	−60	180	56	1								(4)	−60*	130	R	R
																			(2)	−60*	60	3	6
69	L	+	180	60	27	2		180*	60	27	2	L	−		180	60	27	2	(6)	180	180	4	4
																			(4)	180	60	27	2

[a]Rotamers have been rounded to the nearest canonical value using a ±40° cutoff. For angles that deviate greater than 40° from a canonical value, the unrounded eclipsed angle is given. Where there is a distribution of conformers, the number of structures out of 10 that populate each conformer is given in parentheses to the left of the angles. "%" and "Rank" are the percent and the rank ordering of each rotamer in the Protein Data Bank according to the backbone-independent library of Dunbrack (Dunbrack & Cohen, 1997). "R" indicates rare eclipsed angles.

[b]"+" indicates correctly predicted rotamers, "−" indicates incorrectly predicted rotamers, and "?" indicates that the accuracy of the prediction cannot be determined due to ambiguities in the experimental structure. The rotamer that is populated in the majority of the structures (>5) is arbitrarily assigned as the true rotamer value for determination of correct or incorrect prediction.

[c]The program ROC was run 10 times for WT and 1D8 to generate an ensemble of 10 predicted structures for each sequence.

[d]WT experimental data are taken from the WT NMR structure (Cornilescu et al., 1998). "xtal" indicates that the NMR structure differs from both crystal structures 1UBI (Alexeev et al., 1994) and 1UBQ (Vijay-Kumar et al., 1987) at that position, and the crystal structure rotamers are given to the right. "*" indicates angles that are determined by quantitative J coupling measurements.

[e]Core residues that differ between WT and 1D8 are bold in the 1D8 sequence.

[f]Leu13 in 1D8 has no preferred set of rotamers in the experimental ensemble, and the majority of the angles are eclipsed.

χ_1 (Ile13) and one χ_2 (Leu67) rotamer predicted incorrectly (Table 2). Both show discrepancies between the available NMR and crystal structures. The χ_1 of Ile13 is -60 in the NMR structure, eclipsed (130) in both crystal structures, and an intermediate value (60) in the prediction. The predicted χ_2 of Leu67 is in agreement with the two crystal structures but not the NMR structure, in which it is not defined by J coupling data. These side chains have the lowest γ and δ methyl order parameters, respectively, of any core residues in WT (Johnson et al., 1999), explaining the lack of accuracy in the prediction and the discrepancies in the experimental structures. Leu15 also shows increased flexibility—it has a slight tendency to populate a second conformer in the NMR ensemble, occupies an eclipsed rotamer ($\chi_1 = 242$, $\chi_2 = 60$) in the 1UBQ crystal structure (Vijay-Kumar et al., 1987), and has a slightly lower than average side-chain order parameter (Johnson et al., 1999). It is nonetheless predicted correctly. Overall for the very well-packed WT protein, ROC does as good a job at determining core side-chain rotamers as the experimental data and suggests indirectly by its mispredictions which side-chains are more dynamic.

For 1D8, there appears to be substantially more mobility in the core side chains as reflected in the distribution of conformations in the NMR structures (Table 2). Interestingly, there is mobility in the predicted rotamers as well: in contrast to WT for which the same rotamers are predicted in 10 separate simulations, ROC does not converge on the same set of structures for 1D8 (Table 2). ROC correctly predicts 7 of 14 core residues, with one incorrect χ_1 angle (Leu17) and four incorrect χ_2 angles (Leu3, Leu56, Leu61, and Leu69). The two most mobile residues in WT, Leu13 and Ile67, are also dynamic in 1D8, to the extent that the predictions cannot be evaluated. Overall, ROC is worse at predicting the side-chain conformations in 1D8 than WT, and this appears to be due, at least in part, to the higher level of side-chain flexibility in the designed protein.

1D8 has more statistically unfavorable core rotamers

We further evaluated the side-chain conformations by comparing them to a statistically derived rotamer database. Table 2 shows the probability of finding each core residue in its observed conformation for both predicted and experimentally determined structures. The probabilities and rank are based on a backbone-independent rotamer library derived from a statistical analysis of side chains in the Protein Data Bank (PDB) (Dunbrack & Cohen, 1997). The experimental data show that 1D8 has more side chains in statistically less favorable conformations than WT, suggesting a higher level of conformational strain (Fig. 5). This is correlated with the higher level of side-chain mobility relative to the WT protein. Most residues with a single conformer are in the best or second best conformation whereas those that populate unfavorable rotamers tend to sample multiple rotamer states (Fig. 5). The number of statistically less favorable rotamers is a reasonable explanation for the lower stability of 1D8. Increased strain and flexibility of the core side chains could also contribute to loss of stability by disrupting favorable interactions, particularly those which have a steep distance dependence such as van der Waals interactions and H-bonds. The trend is supported by the fact that another designed protein, 1D7, shows intermediate stability between WT and 1D8, and an intermediate level of mobility and strain in its core side chains (Johnson et al., 1999). The ability of ROC to predict side-chain conformation in 1D7 (Johnson et al., 1999) is also intermediate between WT and 1D8, consistent with the observation that predictability breaks down with increased flexibility.

Side-chain conformational strain and flexibility are a probable cause of the minor conformer

There are three core residues in 1D8 (17, 61, and 69) that show a greater level of strain and mobility than in WT. In WT none of these side chains sample more than one rotamer in the ensemble of experimental structures, none show below average side-chain order parameters (Johnson et al., 1999), all are in the first or second most statistically favorable rotamers, and all are predicted correctly by ROC (Table 2). We postulate that this greater level of strain and flexibility in the 1D8 core is related to the exchange behavior of the protein. Many of the side chains in statistically less preferred conformations in 1D8 reside in the same regions that show the greatest chemical shift differences between the major and minor conformations (Fig. 3A,B; Table 2). β-strand five and the preceding turn show by far the largest differences, as well as a loss of H/D exchange protection (Fig. 3C). There is no detailed explanation for why this region is the most affected. One possibility is that it is the most susceptible to perturbation since β5 is partially exposed and unconstrained by a loop or turn at its C-terminal end.

The data also suggest that in ROC calculations of stability, the weighting of intra-side-chain and side-chain–backbone interactions are underestimated relative to side-chain–side-chain interactions. For example, ROC attempts to place three residues (13, 17, and 56) in unfavorable rotamers, presumably because the high energy of these rotamers is overcompensated by good side-chain–side-chain contacts. However, as for 1D7 (Johnson et al., 1999), the experimental data demonstrate the tendency for some side chains to adopt more favorable conformations, particularly those in more ordered regions of the protein (away from the C-termini and loops). Rather than force the side chains into unfavorable rotamers, 1D8 adjusts so that the more favorable rotamers can be utilized, at least part of the time. Apparently, part of the energetically preferable adjustment involves sampling two backbone conformations.

Poor packing is not sufficient to produce a partially folded state of ubiquitin

The altered specificity of 1D8 raises the question: to what extent can the structural specificity of proteins be affected by packing? To answer this question, we investigated the structure of a ubiquitin variant, R7, which has the same core composition as WT but in random order (Lazar et al., 1997). This protein is very poorly packed, and only marginally stable ($\Delta G = 2.0$ kcal/mol for R7, 7.2 kcal/mol for WT), making it an excellent control. Despite this, the $^{15}N/^{1}H$ HSQC spectrum of R7 is as dispersed as that of WT (Fig. 6A) and other ubiquitin core variants (data not shown), and much more dispersed than partially folded or unfolded proteins (Yao et al., 1997; Dyson & Wright, 1998). Complete structural and dynamic information on R7 would be of significant interest, but a challenging task because of its poor solubility (only ~100–200 μM protein samples could be made). Nevertheless, adequate 3D CBCA(CO)NNH and CBCANNH spectra (Bax, 1994) of R7 were obtained for complete backbone $^{1}H/^{15}N/^{13}C\alpha$ and side-chain $^{13}C\beta$ assignments. The fact that all assignments could be made distinguishes R7 from partially folded/molten globule states, which are generally intractable because of low dispersion and severe line-broadening (Dyson & Wright, 1998).

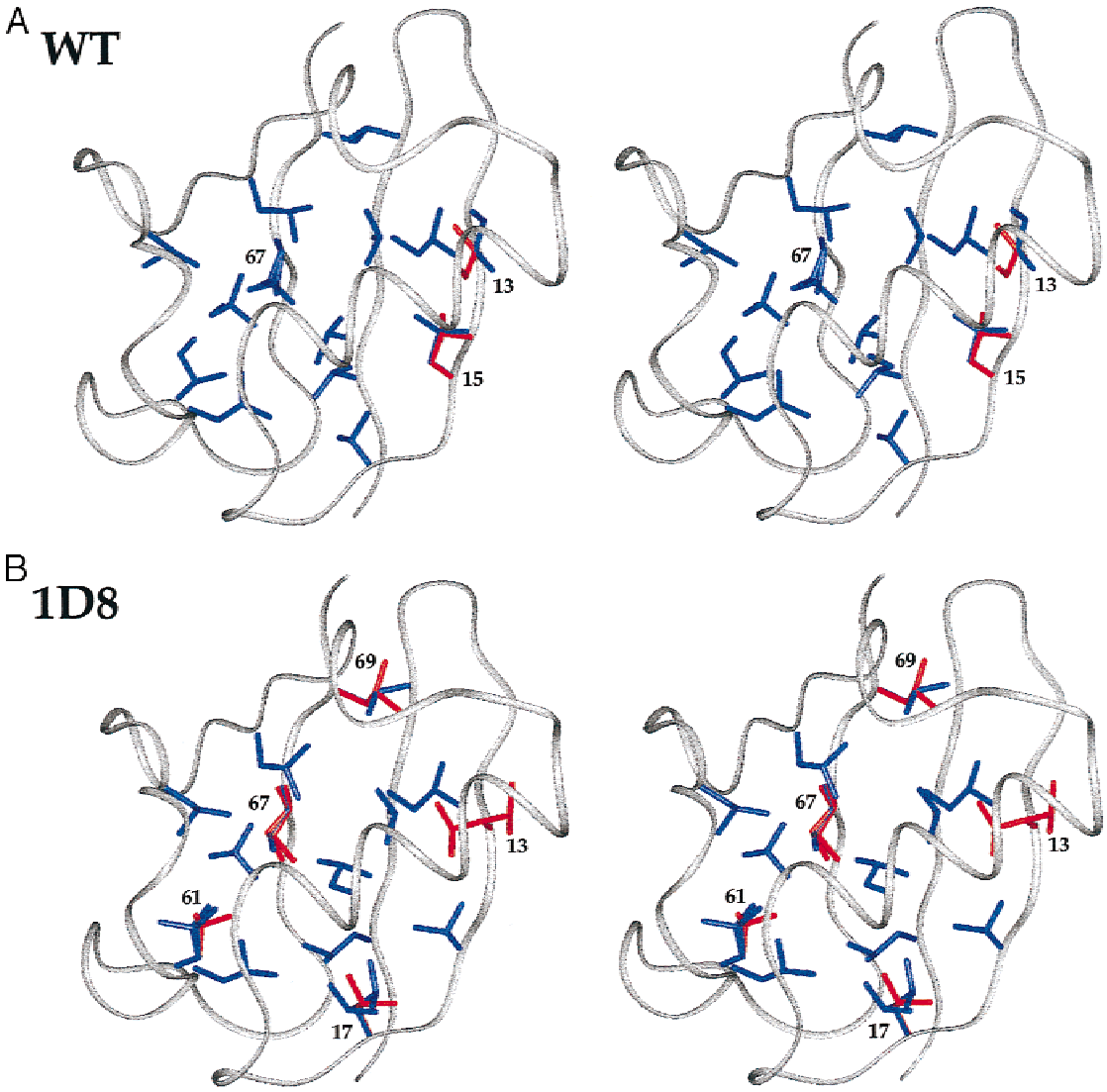

Fig. 5. Experimental core side chains for (**A**) WT and (**B**) 1D8. The angles are those presented in Table 2, and residues that occupy more than one rotamer in the NMR ensembles or are different in the WT NMR and crystal structures are labeled. Side chains occupying rotamers that make up less than 5% of the PDB are colored red, and all other (more statistically favorable) rotamers are colored blue.

Assignments alone provide valuable structural information. ^{13}C chemical shifts of the α- and β-carbons are strongly dependent on the conformation of the protein backbone, and deviation of these chemical shifts from random coil values is an excellent indicator of secondary structure (Spera & Bax, 1991). Residues in helices tend to have positive Cα and negative Cβ chemical shift deviations, while those in β-sheets have negative Cα and positive Cβ deviations. The data for WT and R7 overlap very well (Fig. 6B), even in the absence of definitive trends in some regions of secondary structure. The WT and R7 deviations are as similar as those of WT and 1D8 (data not shown), the folds of which are identical at high resolution (Fig. 1B). This indicates that R7 has a reasonably well-defined structure that is similar to WT ubiquitin. Given the marginal stability and poor packing of this protein relative to the exceptionally stable WT protein, the results strongly suggest that core packing alone does not influence global specificity. This is consistent with other reports, which argue that the pattern of hydrophobic and polar residues is the dominant determinant of fold (Dill, 1990; Kamtekar et al., 1993; Sun et al., 1995; Rojas et al., 1997). Nonetheless, the generality of the R7 result remains to be seen. In oligomeric helical proteins, changes in global specificity have been observed (Harbury et al., 1993; Munson et al., 1996). We suspect that this is because the differences in energy between alternative oligomeric states are small relative to the amount of energy required to interconvert most globular folds, and these energy differences may be well within the range affected by packing interactions. This is supported by the observation of GCN4 variants that exist in equilibrium as dimers and trimers (Gonzalez et al., 1996a, 1996b).

Packing clearly affects the local specificity of 1D8, and this is likely to be true for R7. In fact, extrapolation of the trends observed from a comparison of WT, 1D7, and 1D8 suggests that side-chain flexibility will probably be higher in R7. Because of solubility problems, we have not investigated the presence of

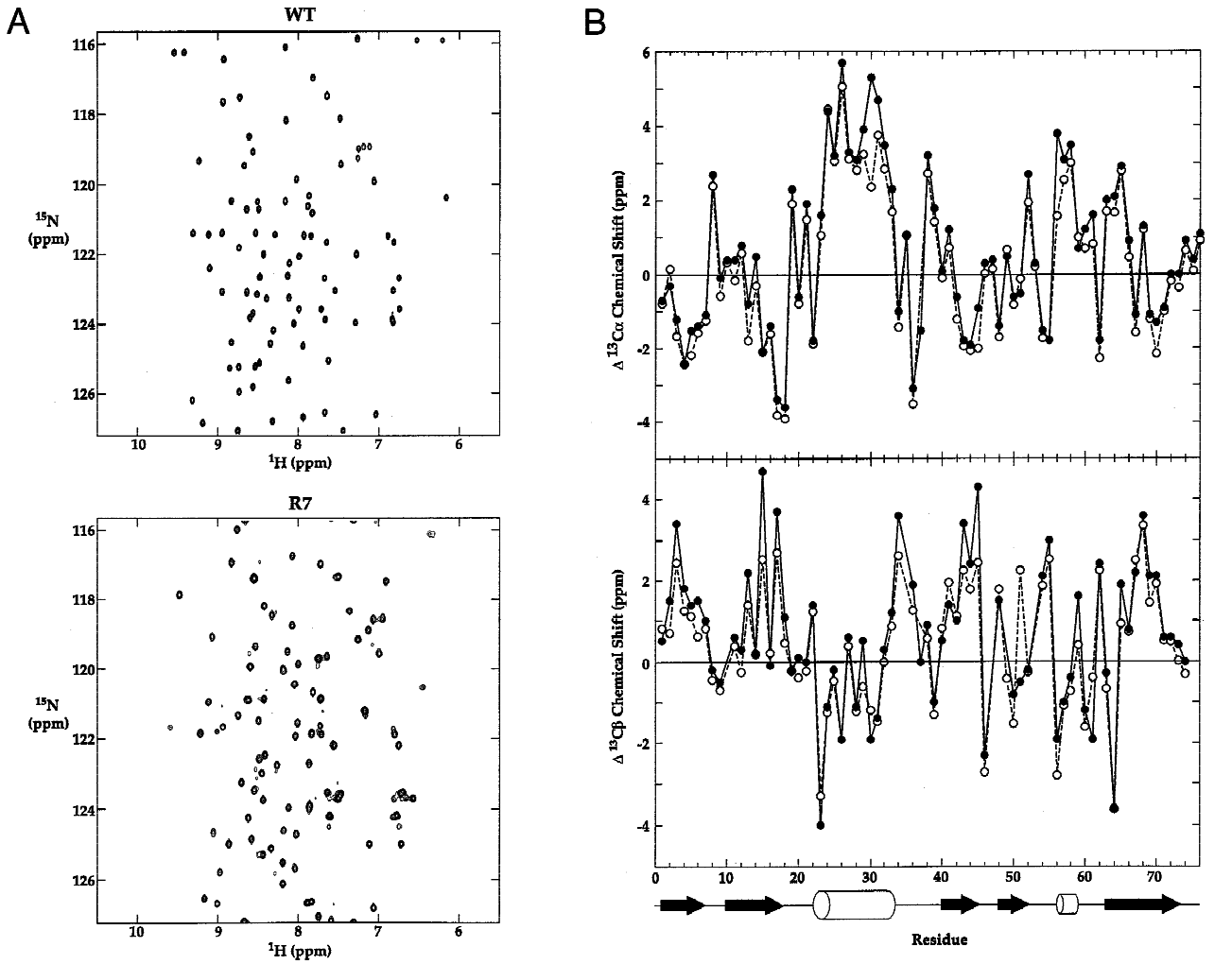

Fig. 6. A: ^{15}N/^{1}H HSQC spectra of WT (top) and R7 (bottom). The ^{15}N spectral width was set to 700 Hz to optimize data collection time, so some of the peaks are aliased. **B:** $^{13}C\alpha$ (top graph) and $^{13}C\beta$ (bottom graph) chemical shift deviations from random coil values for WT (shaded circles, continuous lines) and R7 (open circles, dashed lines). Chemical shift deviations are in parts per million (ppm). Regions of secondary structure are illustrated below the plot.

alternate conformer(s) in R7. However, it is possible that R7 has sufficient flexibility to adjust in multiple ways such that no one conformer is highly populated. Nevertheless, in the context of the rest of the ubiquitin sequence, the presence of very poor packing is not sufficient to change the fold or reduce structural specificity to the level characteristic of molten globules. This suggests that packing can be significantly altered to modulate the dynamic behavior of a protein without drastically affecting its topology or overall well-ordered properties. A key goal for protein design will be to understand how to do this in a predictive way.

Conclusions

1D8 was designed to mimic WT ubiquitin, and the similarity of the structures demonstrates the utility of ROC for protein design. However, careful inspection of the data reveals some subtle but important observations. First, rare rotamers generally appear in the context of side chains that sample multiple conformations, and side chains predicted to be in unfavorable rotamers typically populate a more favorable rotamer or multiple rotamers. This emphasizes the tendency of side chains to adopt the most favorable conformation when possible and suggests that conformational entropy may help offset the effects of strain. Second, strain that would otherwise occur from forcing side chains into poor conformations appears to be partially compensated by sampling more than one conformation. This response of the protein is a unique observation, and together these results contribute new information about the role of the hydrophobic core in protein structure and dynamics. The relationship between side-chain strain and specificity observed in our variant implies that the biological activity of natural proteins may be fine tuned by packing. In future studies it will be important to understand and control these properties for the design of protein–protein interactions and function.

The results also have implications for improvements to design algorithms. When stability and structural rigidity are goals, better

performance may be achieved by restricting acceptable designs to sequences that can accommodate side chains in the most favored rotamers. Furthermore, the data indicate that correlations between predicted and experimentally determined structures, while useful, should be interpreted with caution. The presence of some side chains in multiple rotameric states indicates that ensemble calculations may be more reliable. This is particularly true for lower stability variants, which according to our results are likely to be more flexible and less accurately predicted by a single calculation. Finally, the alternate backbone conformation observed in 1D8 underscores the importance of developing methods that do not rely on a fixed backbone, but rather can sample related structures.

Materials and methods

Ubiquitin proteins

WT, 1D8, and R7 gene construction and protein purification were described previously (Lazar et al., 1997). NMR samples were uniformly labeled with ^{15}N or $^{15}N/^{13}C$ by growth in minimal media containing ^{13}C-glucose and/or ^{15}N-ammonium sulfate as the sole source of carbon and nitrogen. NMR experiments on 1D8 and WT were performed with samples prepared in 25 mM sodium acetate-D_3, 25 mM sodium phosphate, 0.02% sodium azide, 10% D_2O, pH 5.8 at protein concentrations of approximately 2 mM. The R7 samples contained no buffer or salt (only 10% D_2O), pH 5.0, and were approximately 0.2 mM in protein concentration. The temperature for the NMR experiments was 30 °C for 1D8 and WT, and 25 °C for R7.

NMR experiments

Most details of the NMR methodology are similar to those described more completely in previous reports from our laboratory (Johnson et al., 1999; Mizoue et al., 1999). All experiments were carried out on a Bruker DMX600, except for the $^{13}C/^{1}H$ correlation experiment, which was done on a Bruker DRX500. Heteronuclear assignments for 1D8 were obtained using a suite of standard double and triple resonance experiments (Bax, 1994). Chemical shifts were referenced according to the method of Wishart et al. (1995). Structural restraints were obtained from several types of NMR data. NOE distance restraints were obtained from the following experiments: a 3D ^{15}N-separated NOESY-HSQC (Talluri & Wagner, 1996), a 3D ^{13}C-separated NOESY-HSQC (Zuiderweg et al., 1990), and a 4D $^{13}C/^{13}C$-separated HMQC-NOESY-HMQC (Vuister et al., 1993), all using 150 ms mixing times. Quantitative J correlation methods (Bax et al., 1994) provided stereoassignments, as well as ϕ and χ angle restraints. H-bond restraints were derived from slowly exchanging amides identified in an $^{15}N/^{1}H$ HSQC spectrum recorded immediately after resuspension of lyophilized protein in D_2O; a series of such data as a function of time was also used to calculate protection factors (see below). Direct correlations between major and minor conformations in 1D8 were observed using $^{15}N/^{1}H$ and $^{13}C/^{1}H$ HSQC spectra containing a mixing time after the chemical shift evolution period. Two-dimensional difference correlation spectra were obtained by subtracting such experiments from ones in which the mixing time is placed prior to the evolution periods (Wider et al., 1991). Mixing times were varied from 25 to 500 ms.

NMR assignments and structure calculations

Data were processed with the program AZARA (W. Boucher, unpubl. data). A database of chemical shift assignments was made using semi-automated procedures with the program ANSIG3.3 (Kraulis, 1989; Kraulis et al., 1994). NOEs were not assigned but only peak-picked and integrated within ANSIG, then exported and converted into restraint lists in AZARA. The restraint lists were generated by matching the chemical shift of each NOE cross peak with all assignment possibilities within a given tolerance based on the chemical shift database. Two types of restraint tables were output: an unambiguous restraint list (derived from NOE cross peaks that are assignable to a single pair of protons) and an ambiguous restraint file (derived from NOE cross peaks that have multiple assignment possibilities). Initial structures were calculated in X-PLOR (Brünger, 1992) with both unambiguous and ambiguous NOE restraints, treated with r^{-6} summing (Nilges, 1995; Nilges et al., 1997), and dihedral angle restraints. The chirality of nonstereoassigned methyl and methylene groups were allowed to float by setting the force constant for improper angles to zero (Folmer et al., 1997). In addition, random explicit swapping of chirality was performed (Folmer et al., 1997), with acceptance based on a Metropolis criterion (Mizoue et al., 1999). As calculations proceeded, restraint violations and restraints that contributed little to the NOE intensity were gradually discarded with protocols within the ARIA extension of X-PLOR (Nilges, 1995; Nilges et al., 1997). Exchange peaks in 1D8 NOESY spectra were removed subjectively to obtain a structure of the major conformer. In the last few iterations of the calculation, H-bond restraints were introduced. Table 1 shows the distribution of experimental restraints at the beginning and end of the calculations. WT ubiquitin assignments for H/D exchange studies were obtained from Wand and coworkers (Wand et al., 1996). There are two published crystallographic structures of WT, accession codes 1UBQ (Vijay-Kumar et al., 1987) and 1UBI (Alexeev et al., 1994), and a solution structure was obtained through personal communication (Cornilescu et al., 1998). All of these structures are of high quality and are essentially identical. Important discrepancies in core side-chain rotamers between the three WT structures have been noted in the text and Table 2. The 1D8 assignments, restraint lists, and coordinates for the ensemble of structures have been deposited in the Protein Data Bank (accession code 1C3T).

Measurement of protection factors

Amide exchange rates for 1D8 and WT ubiquitin were measured with a series of $^{15}N/^{1}H$ HSQC spectra. Peaks were fit to 2D Gaussians using the program Priism (Chen et al., 1996). Exchange rates were calculated by fitting peak heights to a decaying exponential with a baseline. Protection factors were calculated from the equation:

$$P = k_{rc}/k_{obs}$$

where k_{rc} is the exchange rate expected for a random coil and k_{obs} is the measured exchange rate. k_{rc} is calculated using the method of Englander and colleagues (Bai et al., 1993), taking into account the contributions from neighboring side chains, pH, and temperature.

Rotamer analysis

Prediction of core side-chain structure for WT and 1D8 was performed with ROC (Desjarlais & Handel, 1995), using version

ROC* (Lazar et al., 1997). Predictions were obtained by fixing the core composition and allowing only side-chain conformation to mutate during ROC calculations. ROC was run with 10 supercycles of 300 rounds of "evolution," generating an ensemble of 10 structures for each protein. The template for the predictions was the crystal structure 1UBI (Alexeev et al., 1994). The output from each run consists of a list of energetically favorable cores with the 1D8 or WT sequence, but different rotamer conformations and calculated energies. Predicted and experimental rotamers in Table 2 were assigned to −60, 60, or 180 if they were within ±40° of the canonical value. When there was a distribution between two conformers in the predicted structure or the ensemble of NMR structures, the rotamer, which was populated in the majority of the structures (>5), was arbitrarily assigned as the true rotamer value for assignment of the prediction as correct or incorrect. Statistical analysis of side-chain conformations for the predicted and experimentally determined structures was performed with the backbone-independent library of Dunbrack (Dunbrack & Cohen, 1997) (URL:www.fccc.edu/research/labs/dunbrack/sidechain.html).

Acknowledgments

We thank Ad Bax and John Marquardt for providing the WT NMR coordinates, Susan Marqusee and Dave Wemmer for DRX500 NMR time, and Casey Owens for assistance in assigning R7. T.M.H. is an NSF Young investigator and J.R.D. was a fellow of the Jane Coffin Childs Memorial Fund for Medical Research. This work was supported by an NSF grant to T.M.H. and an NSF Graduate Research Fellowship to G.A.L.

References

Alexeev D, Bury SM, Turner MA, Ogunjobi OM, Muir TW, Ramage R, Sawyer L. 1994. Synthetic, structural and biological studies of the ubiquitin system: Chemically synthesized and native ubiquitin fold into identical three-dimensional structures. *Biochem J 299*:159–163.

Anderson DH, Weiss MS, Eisenberg D. 1997. Charges, hydrogen bonds, and correlated motions in the 1 Å resolution refined structure of the mating pheromone Er-1 from *Euplotes raikovi*. *J Mol Biol 273*:479–500.

Bai Y, Englander JJ, Mayne L, Milne JS, Englander SW. 1995. Thermodynamic parameters from hydrogen exchange measurements. *Methods Enzymol 259*: 344–356.

Bai Y, Milne JS, Mayne L, Englander SW. 1993. Primary structure effects on peptide group hydrogen exchange. *Proteins 17*:75–86.

Baldwin EP, Hajiseyedjavadi O, Baase WA, Matthews BW. 1993. The role of backbone flexibility in the accommodation of variants that repack the core of T4 lysozyme. *Science 262*:1715–1718.

Bax A. 1994. Multidimensional nuclear magnetic resonance methods for protein studies. *Curr Opin Struct Biol 4*:738–744.

Bax A, Vuister GW, Grzesiek S, Delaglio F, Wang AC, Tschudin R, Zhu G. 1994. Measurement of homo- and heteronuclear J couplings from quantitative J correlation. *Methods Enzymol 239*:79–105.

Brünger AT. 1992. *X-PLOR manual, version 3.0*. New Haven, CT: Yale University Press.

Chatfield DC, Szabo A, Brooks BR. 1998. Molecular dynamics of staphylococcal nuclease: Comparison of simulation with N-15 and C-13 NMR relaxation data. *J Am Chem Soc 120*:5301–5311.

Chen H, Hughes DD, Chan TA, Sedat JW, Agard DA. 1996. IVE (Image Visualization Environment): A software platform for all three-dimensional microscopy applications. *J Struct Biol 116*:56–60.

Cornilescu G, Marquardt JL, Ottiger M, Bax A. 1998. Validation of protein structure from anisotropic carbonyl chemical shifts in a dilute liquid crystalline phase. *J Am Chem Soc 120*:6836–6837.

Dahiyat BI, Mayo SL. 1997. *De novo* protein design: Fully automated sequence selection. *Science 278*:82–87.

Desjarlais JR, Handel TM. 1995. *De novo* design of the hydrophobic cores of proteins. *Protein Sci 4*:2006–2018.

Dill KA. 1990. Dominant forces in protein folding. *Biochemistry 29*:7133–7155.

Dunbrack RL, Cohen FE. 1997. Bayesian statistical analysis of protein side-chain rotamer preferences. *Protein Sci 6*:1661–1681.

Dyson HJ, Wright PE. 1998. Equilibrium NMR studies of unfolded and partially folded proteins. *Nat Struct Biol 5 Suppl*:499–503.

Folmer RH, Hilbers CW, Konings RN, Nilges M. 1997. Floating stereospecific assignment revisited: Application to an 18 kDa protein and comparison with J-coupling data. *J Biomol NMR 9*:245–258.

Gonzalez LJ, Plecs JJ, Alber T. 1996a. An engineered allosteric switch in leucine-zipper oligomerization. *Nat Struct Biol 3*:510–515.

Gonzalez LJ, Woolfson DN, Alber T. 1996b. Buried polar residues and structural specificity in the GCN4 leucine zipper. *Nat Struct Biol 3*:1011–1018.

Harata K, Abe Y, Muraki M. 1999. Crystallographic evaluation of internal motion of human alpha-lactalbumin refined by full-matrix least-squares method. *J Mol Biol 287*:347–358.

Harbury PB, Zhang T, Kim PS, Alber T. 1993. A switch between two-, three-, and four-stranded coiled coils in GCN4 leucine zipper mutants. *Science 262*:1401–1407.

Hellinga HW. 1998. The construction of metal centers in proteins by rational design. *Folding Design 3*:R1–R8.

Jackson SE, Moracci M, elMasry N, Johnson CM, Fersht AR. 1993. Effect of cavity-creating mutations in the hydrophobic core of chymotrypsin inhibitor 2. *Biochemistry 32*:11259–11269.

Johnson EC, Lazar GA, Desjarlais JR, Handel TM. 1999. Solution structure and dynamics of a designed hydrophobic core variant of ubiquitin. *Struct Fold Design 7*:967–976.

Kamtekar S, Schiffer JM, Xiong H, Babik JM, Hecht MH. 1993. Protein design by binary patterning of polar and nonpolar amino acids. *Science 262*:1680–1685.

Kortemme T, Ramirez-Alvarado M, Serrano L. 1998. Design of a 20-amino acid, three-stranded β-sheet protein. *Science 281*:253–256.

Kraulis PJ. 1989. Ansig—A program for the assignment of protein H-1 2D-NMR spectra by interactive computer graphics. *J Magn Reson 84*:627–633.

Kraulis PJ, Domaille PJ, Campbell-Burk SL, Van Aken T, Laue ED. 1994. Solution structure and dynamics of ras p21.GDP determined by heteronuclear three- and four-dimensional NMR spectroscopy. *Biochemistry 33*: 3515–3531.

Laskowski RA, Rullmann JA, MacArthur MW, Kaptein R, Thornton JM. 1996. AQUA and PROCHECK-NMR: Programs for checking the quality of protein structures solved by NMR. *J Biomol NMR 8*:477–486.

Lazar GA, Desjarlais JR, Handel TM. 1997. *De novo* design of the hydrophobic core of ubiquitin. *Protein Sci 6*:1167–1178.

Lazar GA, Handel TM. 1998. Hydrophobic core packing and protein design. *Curr Opin Chem Biol 2*:675–679.

Lim WA, Hodel A, Sauer RT, Richards FM. 1994. The crystal structure of a mutant protein with altered but improved hydrophobic core packing. *Proc Natl Acad Sci USA 91*:423–427.

Lim WA, Sauer RT. 1991. The role of internal packing interactions in determining the structure and stability of a protein. *J Mol Biol 219*:359–376.

Lipari G, Szabo A. 1982. Model-free approach to the interpretation of nuclear magnetic resonance relaxation in macromolecules. I. Theory and range of validity. *J Am Chem Soc 104*:4546–4559.

Miller DW, Agard DA. 1999. Enzyme specificity under dynamic control: A normal mode analysis of alpha-lytic protease. *J Mol Biol 286*:267–278.

Mizoue LS, Bazan JF, Johnson EC, Handel TM. 1999. Solution structure and dynamics of the CX_3C chemokine domain of fractalkine and its interaction with an N-terminal fragment of CX_3CR1. *Biochemistry 38*:1402–1414.

Munson M, Balasubramanian S, Fleming KG, Nagi AD, O'Brien R, Sturtevant JM, Regan L. 1996. What makes a protein a protein? Hydrophobic core designs that specify stability and structural properties. *Protein Sci 5*:1584–1593.

Nilges M. 1995. Calculation of protein structures with ambiguous distance restraints. Automated assignment of ambiguous NOE cross peaks and disulphide connectivities. *J Mol Biol 245*:645–660.

Nilges M, Macias MJ, O'Donoghue SI, Oschkinat H. 1997. Automated NOESY interpretation with ambiguous distance restraints: The refined NMR solution structure of the pleckstrin homology domain from beta-spectrin. *J Mol Biol 269*:408–422.

Palmer AG. 1997. Probing molecular motion by NMR. *Curr Opin Struct Biol 7*:732–737.

Palmer AG, Williams J, McDermott A. 1996. Nuclear magnetic resonance studies of biopolymer dynamics. *J Phys Chem 100*:13293–13310.

Philippopoulos M, Lim C. 1999. Exploring the dynamic information content of a protein NMR structure: Comparison of a molecular dynamics simulation with the NMR and X-ray structures of *Escherichia coli* ribonuclease HI. *Proteins 36*:87–110.

Rader SD, Agard DA. 1997. Conformational substates in enzyme mechanism: The 120 K structure of alpha-lytic protease at 1.5 Å resolution. *Protein Sci 6*:1375–1386.

Rojas NR, Kamtekar S, Simons CT, McLean JE, Vogel KM, Spiro TG, Farid

RS, Hecht MH. 1997. *De novo* heme proteins from designed combinatorial libraries. *Protein Sci 6*:2512–2524.
Spera S, Bax A. 1991. Empirical correlation between protein backbone conformation and C-alpha and C-beta C-13 nuclear magnetic resonance chemical shifts. *J Am Chem Soc 113*:5490–5492.
Starich MR, Wikstrom M, Schumacher S, Arst HNJ, Gronenborn AM, Clore GM. 1998. The solution structure of the leu22 → val mutant AREA DNA binding domain complexed with a TGATAG core element defines a role for hydrophobic packing in the determination of specificity. *J Mol Biol 277*:621–634.
Sun S, Brem R, Chan HS, Dill KA. 1995. Designing amino acid sequences to fold with good hydrophobic cores. *Protein Eng 8*:1205–1213.
Talluri S, Wagner G. 1996. An optimized 3D NOESY-HSQC. *J Magn Reson Series B 112*:200–205.
Vijay-Kumar S, Bugg CE, Cook WJ. 1987. Structure of ubiquitin refined at 1.8 Å resolution. *J Mol Biol 194*:531–544.
Vuister GW, Clore GM, Gronenborn AM, Powers R, Garrett DS, Tschudin R, Bax A. 1993. Increased resolution and improved spectral quality in four-dimensional $^{13}C/^{13}C$-separated HMQC-NOESY-HMQC spectra using pulsed field gradients. *J Magn Reson B 101*:210–213.
Walsh STR, Cheng W, Bryson JW, Roder H, Degrado WF. 1999. Solution structure and dynamics of a de novo designed three-helix bundle protein. *Proc Natl Acad Sci USA 96*:5486–5491.
Wand AJ, Urbauer JL, McEvoy RP, Bieber RJ. 1996. Internal dynamics of human ubiquitin revealed by ^{13}C-relaxation studies of randomly fractionally labeled protein. *Biochemistry 35*:6116–6125.
Wider G, Neri D, Wüthrich K. 1991. Studies of slow conformational equilibria in macromolecules by exchange of heteronuclear longitudinal 2-spin-order in a 2D difference correlation experiment. *J Biomol NMR 1*:93–98.
Wishart DS, Bigam CG, Yao J, Abildgaard F, Dyson HJ, Oldfield E, Markley JL, Sykes BD. 1995. ^{1}H, ^{13}C, and ^{15}N chemical shift referencing in biomolecular NMR. *J Biomol NMR 6*:135–140.
Yao J, Dyson HJ, Wright PE. 1997. Chemical shift dispersion and secondary structure prediction in unfolded and partly folded proteins. *FEBS Lett 419*:285–289.
Zuiderweg ERP, McIntosh LP, Dahlquist FW, Fesik SW. 1990. 3-Dimensional C-13-resolved proton NOE spectroscopy of uniformly C-13-labeled proteins for the NMR assignment and structure determination of larger molecules. *J Magn Reson 86*:210–216.